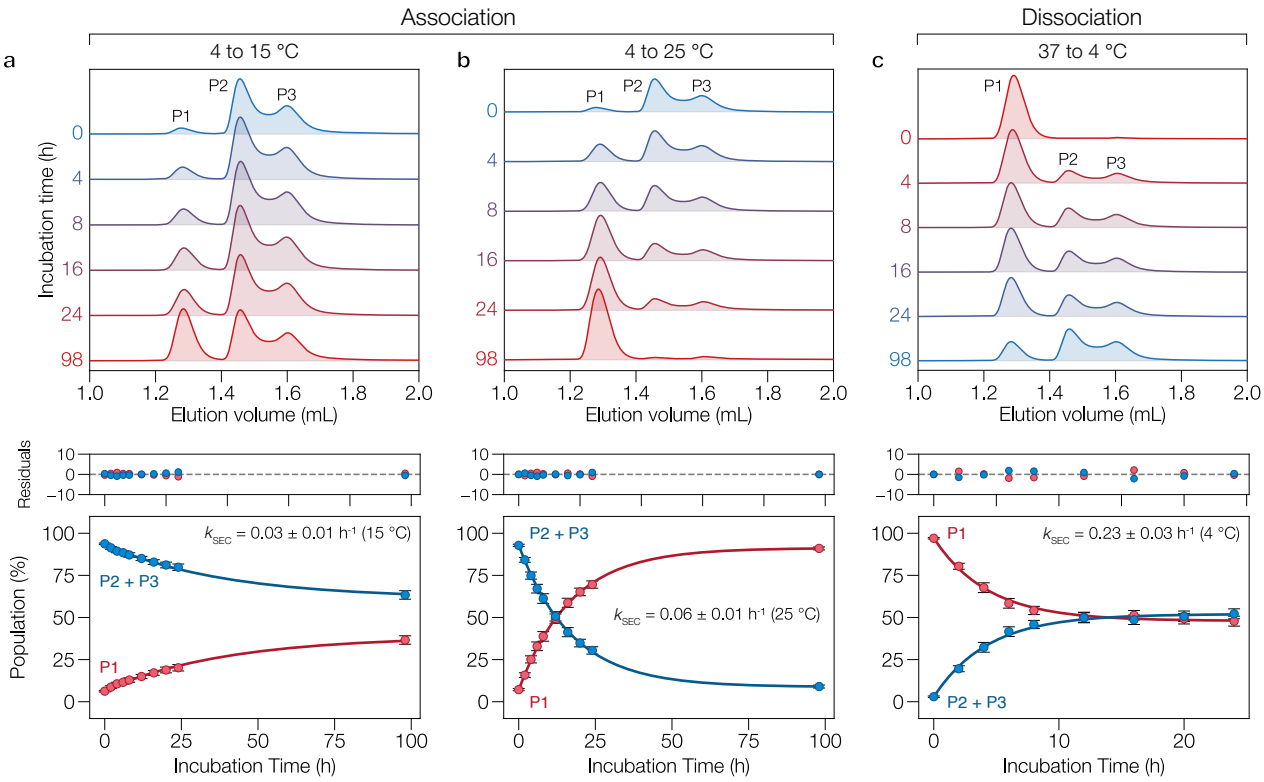

Supplementary Figure 1. Size-exclusion chromatograms examining the temperature-dependent association and dissociation of Bpa. Bpa equilibrated at 4°C was incubated at either (**a**) 15 °C or (**b**) 25 °C to monitor Bpa association; (**c**) Bpa equilibrated at 37 °C was incubated at 4 °C to monitor dissociation. The high-molecular weight (MW) species is denoted as P1 (peak 1), while the two lower-MW species are denoted as P2 and P3 (peaks 2 and 3). Changes in the fractional populations of the P1 (red) and P2+P3 (blue) species for each time course are shown below the corresponding chromatograms. The first-order rate for each time course obtained by a fit to an exponential decay model along with the residuals are displayed. Source data are provided as a Source Data file.

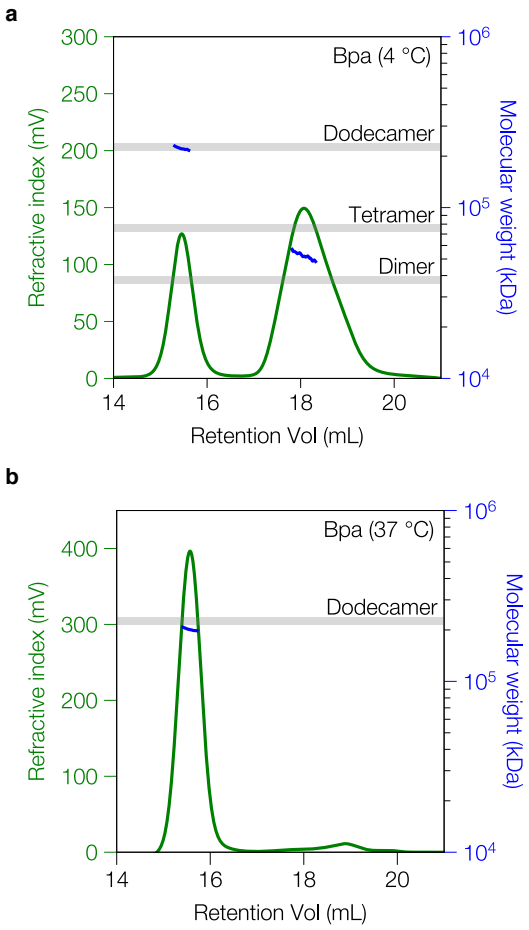

Supplementary Figure 2. SEC-MALS analysis of apo Bpa at 4 and 37 °C. (**a**) Bpa $_{WT}$ incubated at 4 °C. Two distinct peaks are observed, a well-resolved peak corresponding to dodecameric Bpa and a broad peak corresponding to trimeric Bpa. The grey bar indicates the expected molecular weight ± 5%. (**b**) Bpa $_{WT}$ incubated at 37 °C and analyzed at 20 °C. A single predominant peak corresponding to dodecameric Bpa is observed. The left y-axis and green trace represent the refractive index signal, which reflects protein concentration, while the right y-axis and blue trace indicate the estimated molecular weight. Grey bars denote ±5% of the expected molecular weight for each indicated oligomeric species. An OMNISEC multi-detector SEC system (Malvern Panalytical, United Kingdom) fitted with an OMNISEC RESOLVE and OMNISEC REVEAL modules was used. Source data are provided as a Source Data file.

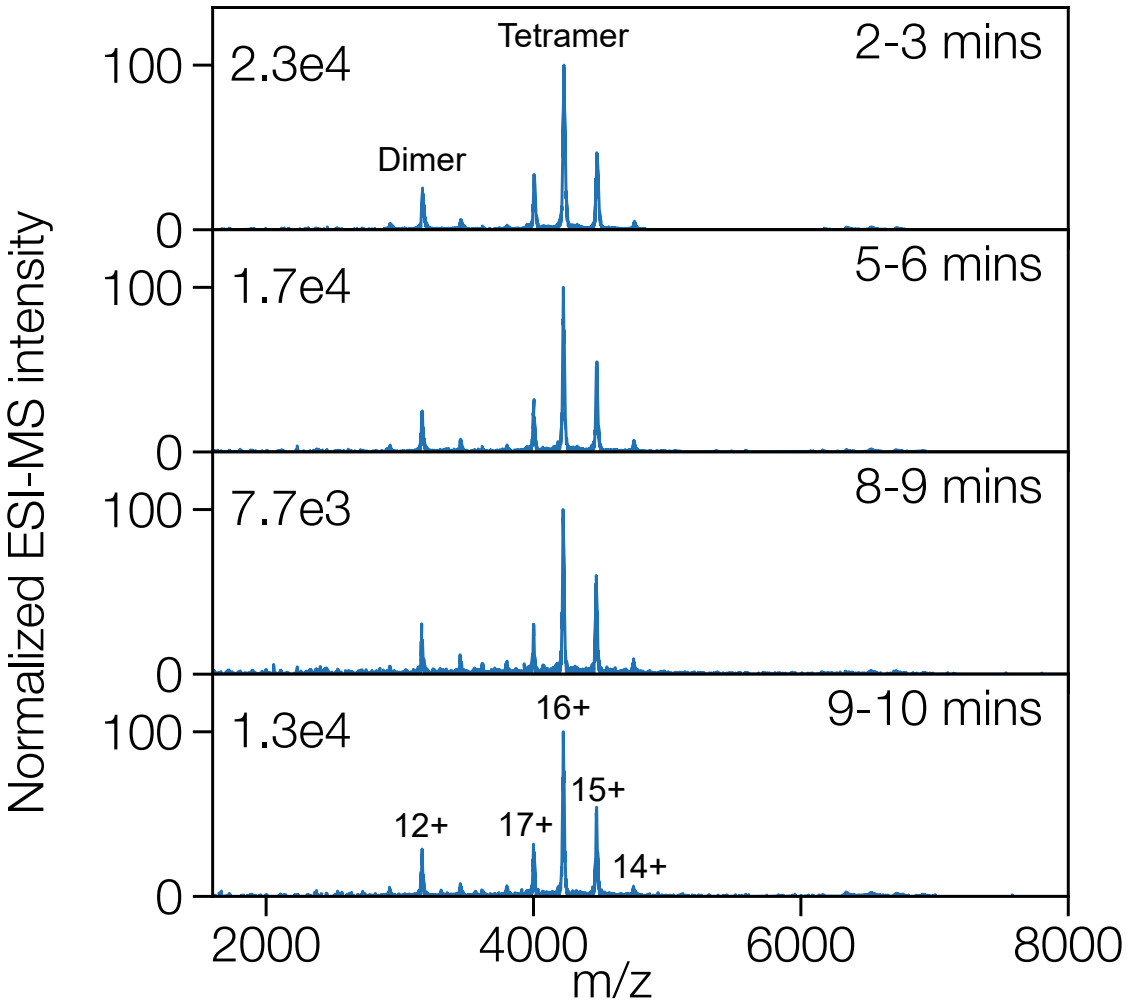

Supplementary Figure 3. Temperature changes during native MS do not alter Bpa oligomeric distribution. Segmenting the native MS acquisition for unassembled Bpa shows stable population distributions across measurement time, indicating prolonged measurements did not perturb oligomeric states; prominent species and charge states are annotated.

Supplementary Figure 4. Bpa peptide coverage map in HDX-MS experiments. Peptide coverage for Bpa after online digestion using nepenthesin II for pulsed HDX-MS experiments. After filtering using the parameters listed, 87 peptides with quantifiable deuterium uptake remained, corresponding to a sequence coverage of 100% and a peptide redundancy level of 5.60.

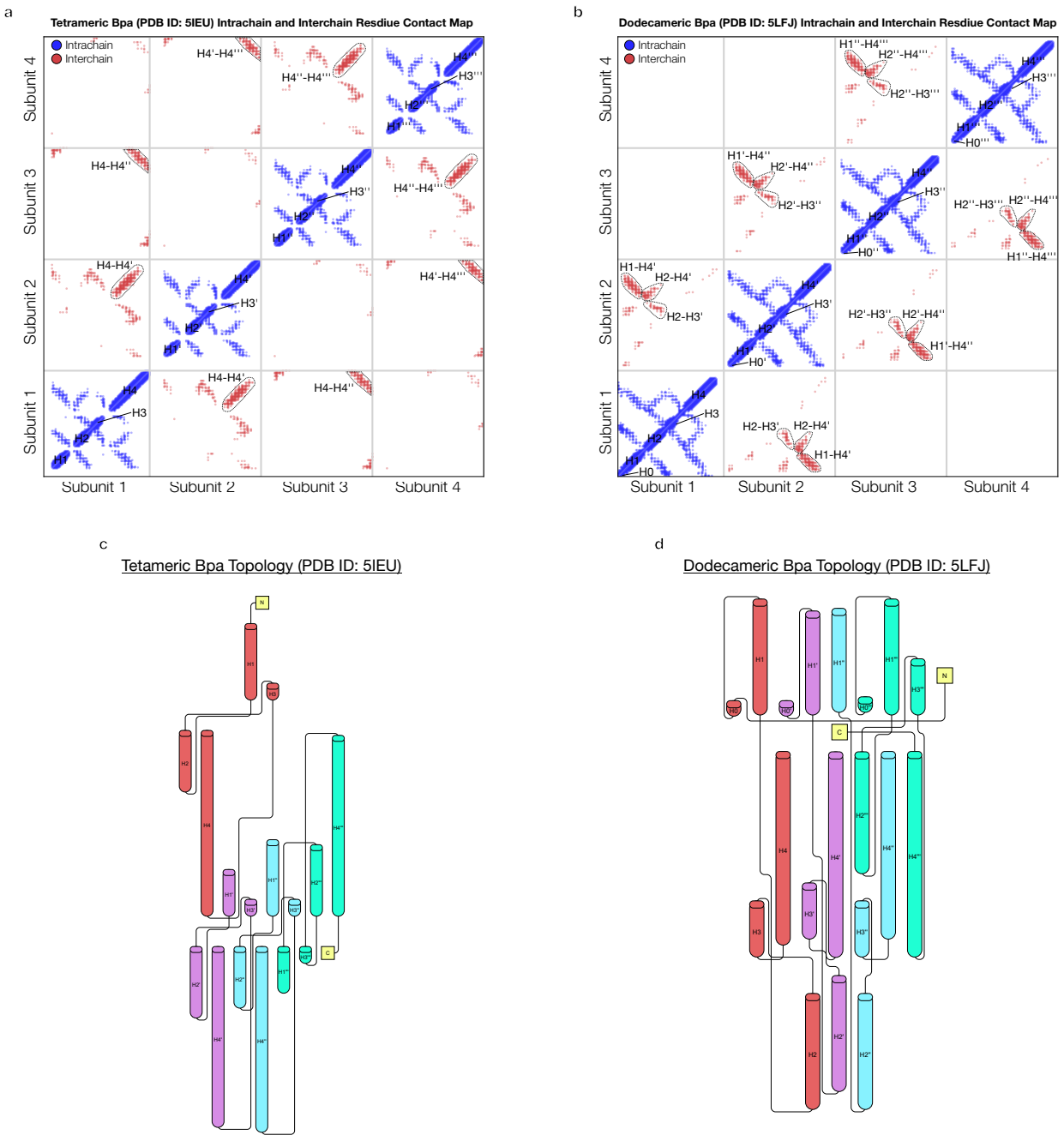

Supplementary Figure 5. Intrachain and interchain residue contacts in dodecameric and tetrameric Bpa. Residue-residue contacts are shown for each subunit of Bpa within the **(a)** tetrameric (PDB ID: 5IEU) or **(b)** dodecameric (PDB ID: 5LFJ) assemblies. Intrachain contacts are shown in blue and interchain contacts are shown in

red. Prominent interactions between secondary structure elements of adjacent subunits are labelled. Protein topology diagram for the **(c)** tetrameric (PDB ID: 5IEU) or **(d)** the dodecameric (PDB ID: 5LFJ) forms. These figures were generated using Pro-origami[1].

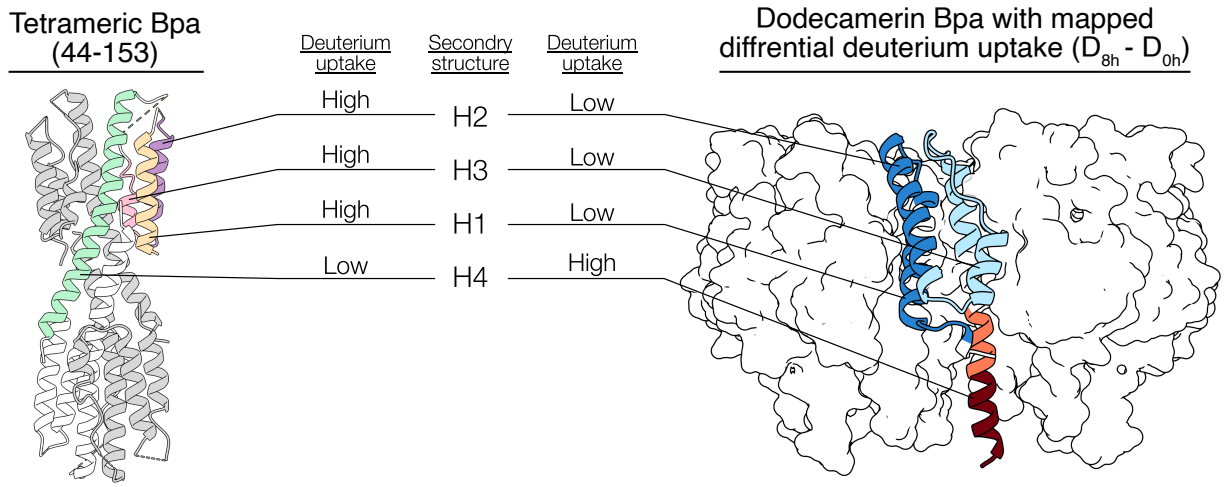

Supplementary Figure 6. Structural comparison of tetrameric and dodecameric Bpa assemblies. Left: Crystal structure of the tetrameric Bpa construct (residues 44–153; PDB: 5IEU)[2], shown as a cartoon with each helix individually colored. Right: Dodecameric Bpa (PDB: 5LFJ)[3], shown as a surface representation, with one subunit displayed as a cartoon and colored according to differential deuterium uptake after 8 hours of assembly (from HDX-MS). Increased deuterium uptake in helix H4 in the dodecamer reflects loss of protection due to conformational rearrangement. In the tetramer, H4 forms a tightly packed inter-subunit interface (green), leading to strong protection. In contrast, helices H1, H2, and H3 are solvent exposed in the tetramer and exchange rapidly, but become buried and protected upon dodecamer formation as they are sequestered between adjacent Bpa subunits.

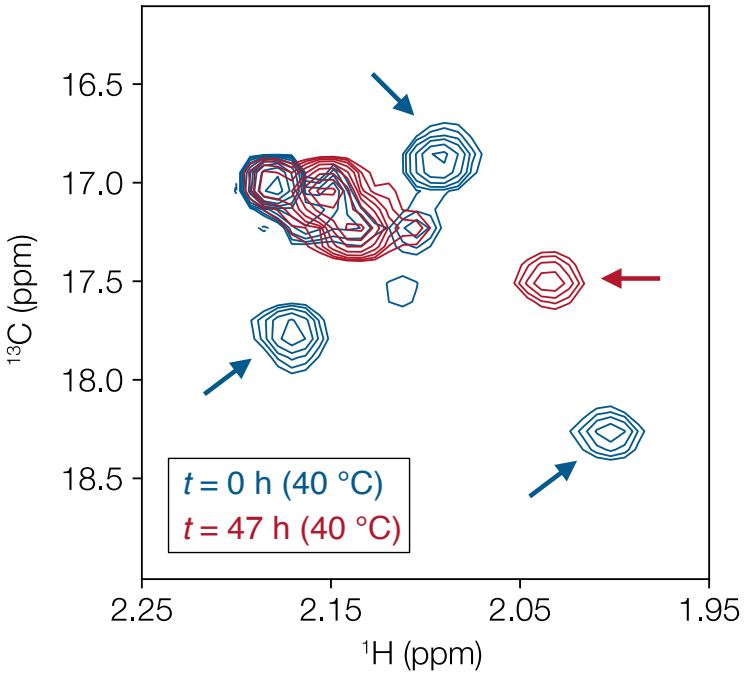

Supplementary Figure 7. NMR probes used for the measurement of the kinetics of tetramer-dodecamer interconversion and the establishment of diffusion rates of each species. We performed a kinetic experiment to follow the disappearance of the low-temperature tetramer and buildup of dodecameric Bpa NMR signals by recording a series of HMQC spectra at 40 °C. Overlay of ^{1}H-^{13}C HMQC spectra of ILVM-labelled Bpa, focusing on the Met region of the data set, at t = 0 (immediately after equilibration at 4 °C; blue) and at t = 47 h (red). The arrows indicate which isolated peaks were used in our analyses.

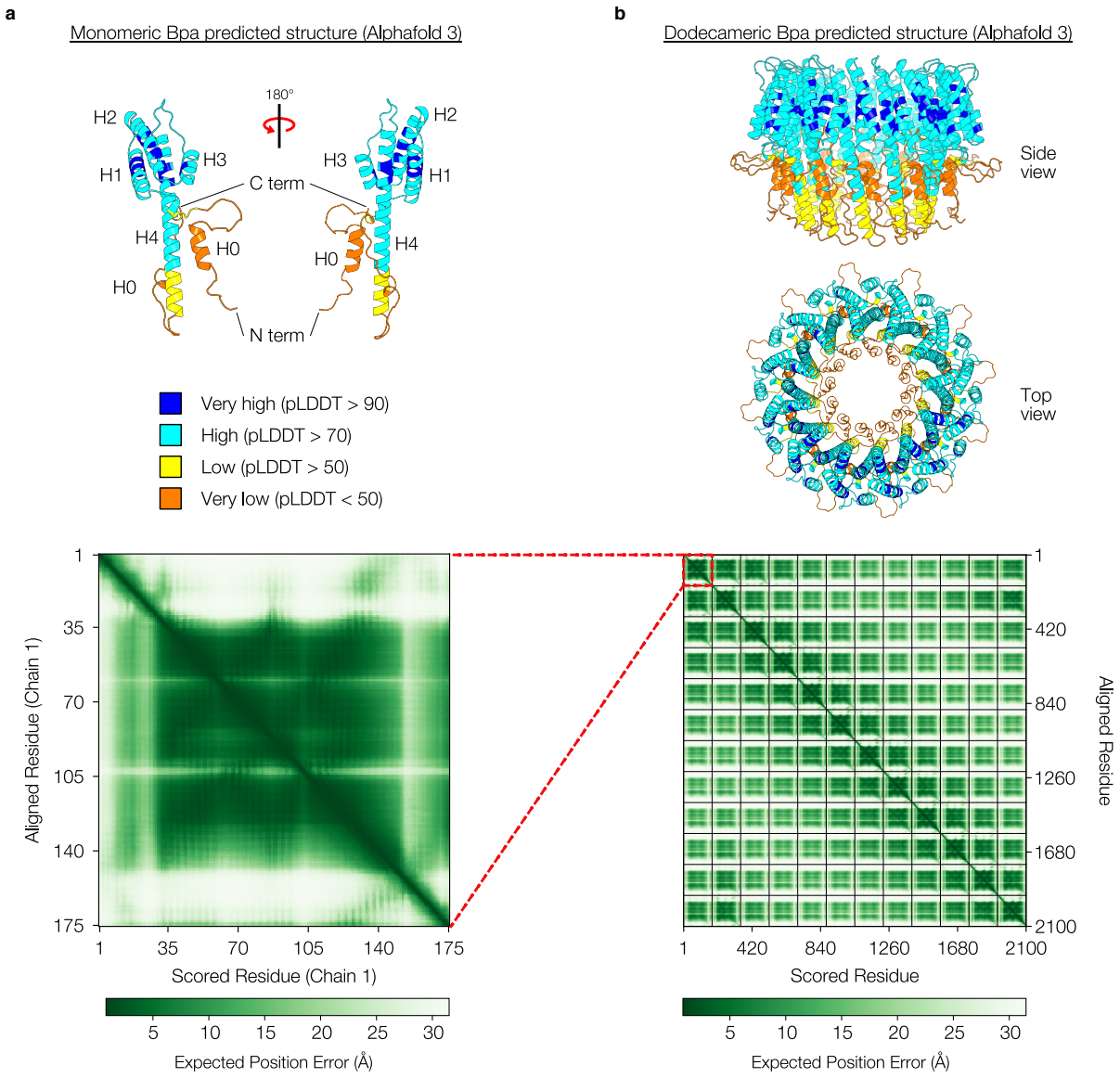

Supplementary Figure 8. AlphaFold3 predicts that the N and C termini of Bpa are unstructured. (a) Cartoon representation of a Bpa monomer predicted by AlphaFold 3 (AF-P9WKX3-F1). The structure is coloured according to the pLDDT score which is indicative of the prediction confidence. All elements of secondary structure and each terminus are labelled; and (b) Predicated aligned error (PAE) plot for the AlphaFold3 predicted structure.

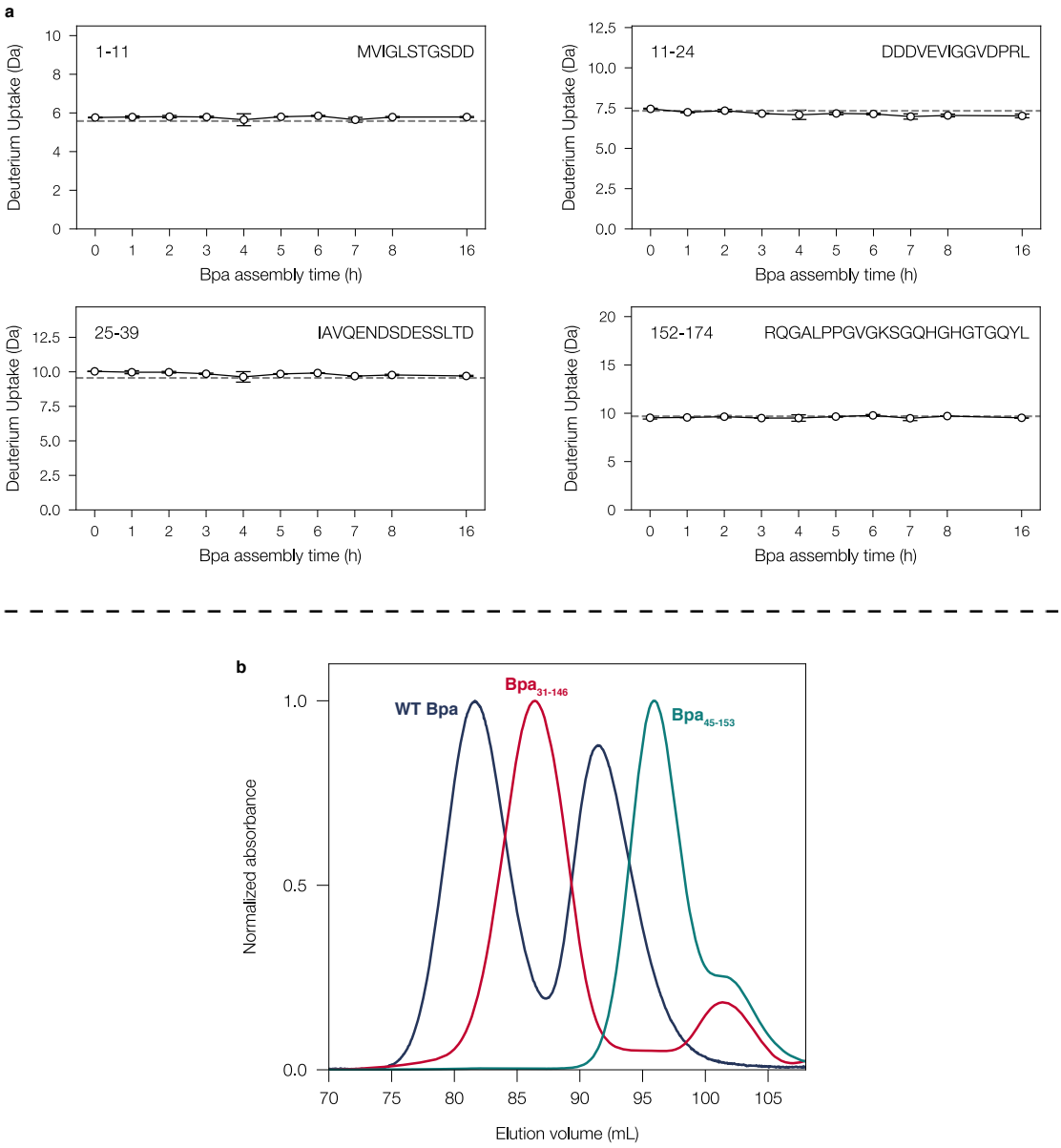

Supplementary Figure 9. Deuterium uptake plots for disordered N- and C-terminal peptides. (a) N- and C-terminal peptides become fully deuterated after a 10-second exposure to D_2O with no observable kinetics as a function of Bpa assembly time indicating unstructured termini. The dashed horizontal line indicates the fully deuterated control. The start and end residue numbers and peptide sequence are indicated in the top left and right corners of each plot, respectively; and (b) SEC profiles of WT Bpa, Bpa $_{31\text{-}146}$, and Bpa $_{45\text{-}153}$. Source data are provided as a Source Data file.

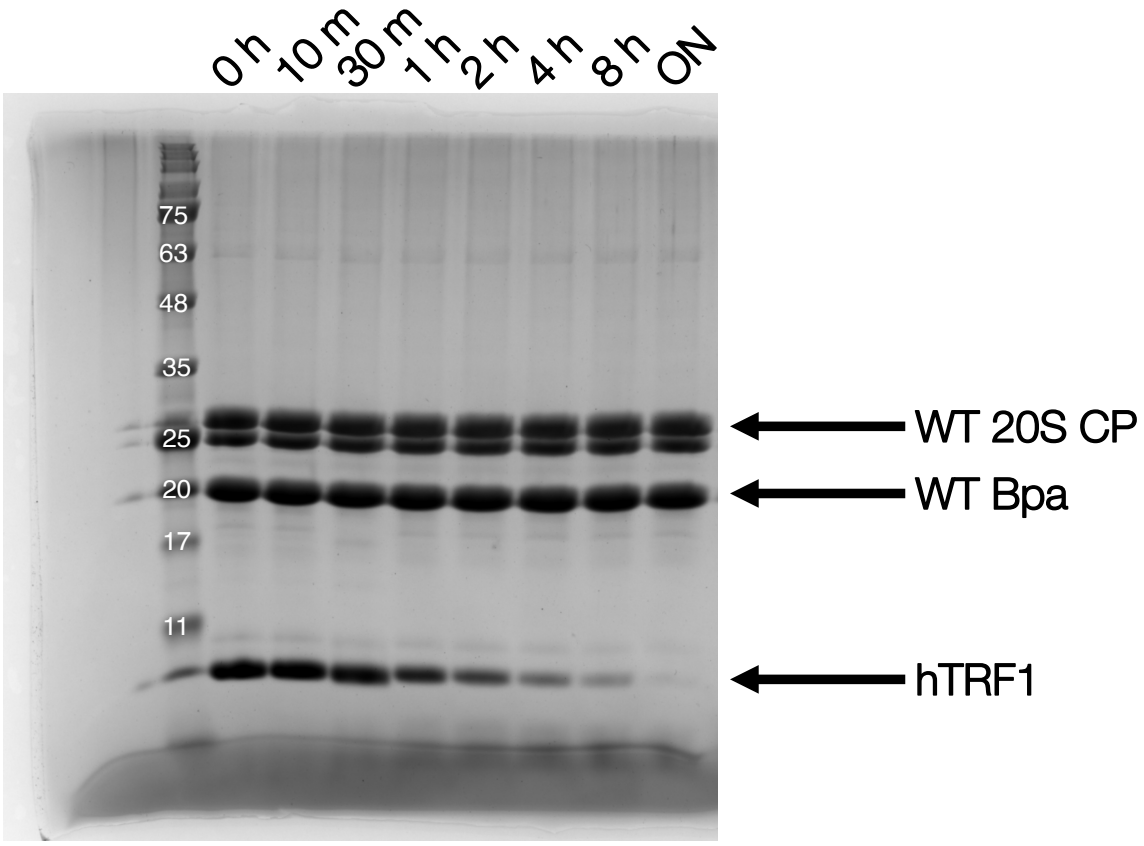

Supplementary Figure 10. Bpa-mediated proteasomal degradation of non-native substrate hTRF1. All components (WT Bpa, WT 20S CP, hTRF1) were combined and incubated at 37 °C for 48 hours. Aliquots were taken at discrete time points and quenched. Reaction protein concentrations were 0.14 μM 20S CP, 0.8 μM Bpa (dodecamer), and 10 μM hTRF1. Source data are provided as a Source Data file.

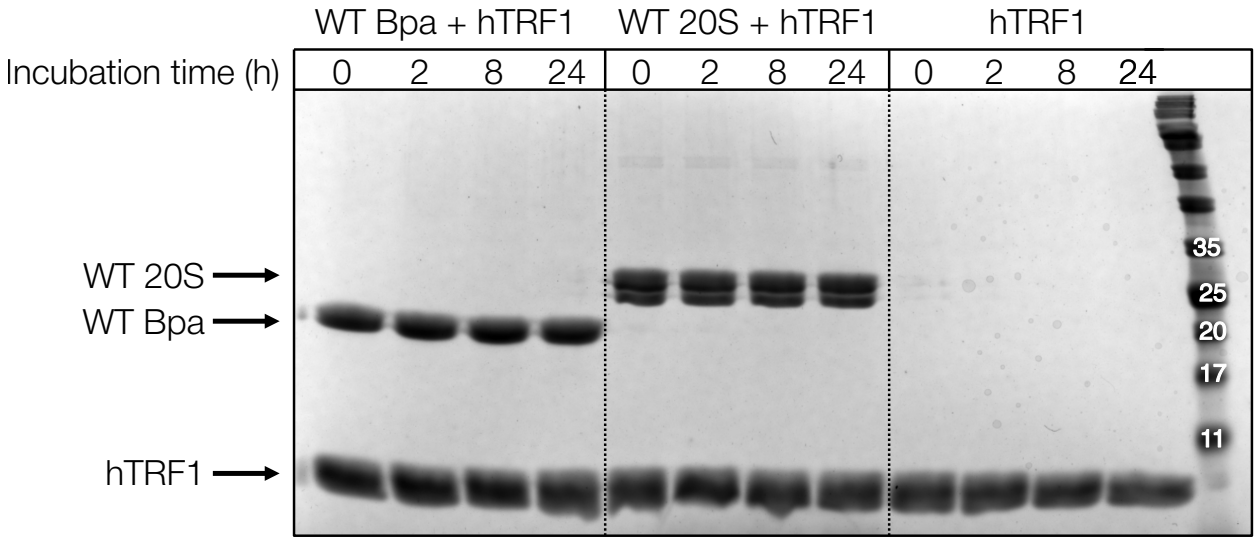

Supplementary Figure 11. hTRF1 does not undergo degradation when incubated individually with WT Bpa or WT 20S. WT Bpa + hTRF1, WT 20S CP + hTRF1, and hTRF1 were incubated at 37 °C for 24 hours. Aliquots were taken at discrete time points and quenched. Reaction protein concentrations were 0.14 μM 20S CP, 0.8 μM Bpa (dodecamer), and 10 μM hTRF1. Source data are provided as a Source Data file.

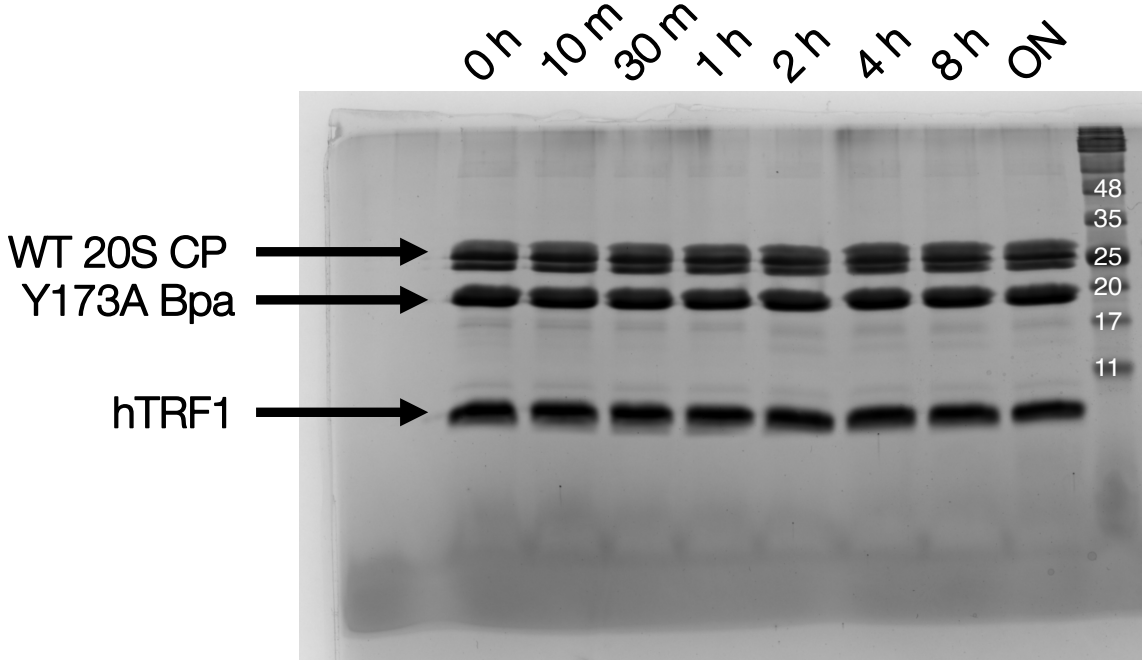

Supplementary Figure 12. The Y173A substitution in Bpa abrogates association with 20S CP resulting in lack of hTRF1 degradation. Lack of degradation when Y173A Bpa is used shows that GQYL-mediated interaction between WT Bpa-20S (Fig. S5) is required for degradation to proceed. All components (Y173A Bpa, WT 20S CP, hTRF1) were combined and incubated at 37 °C for 48 hours. Aliquots were taken at discrete time points and quenched. Reaction protein concentrations were 0.14 μM 20S CP, 0.8 μM Bpa (dodecamer), and 10 μM hTRF1. Source data are provided as a Source Data file.

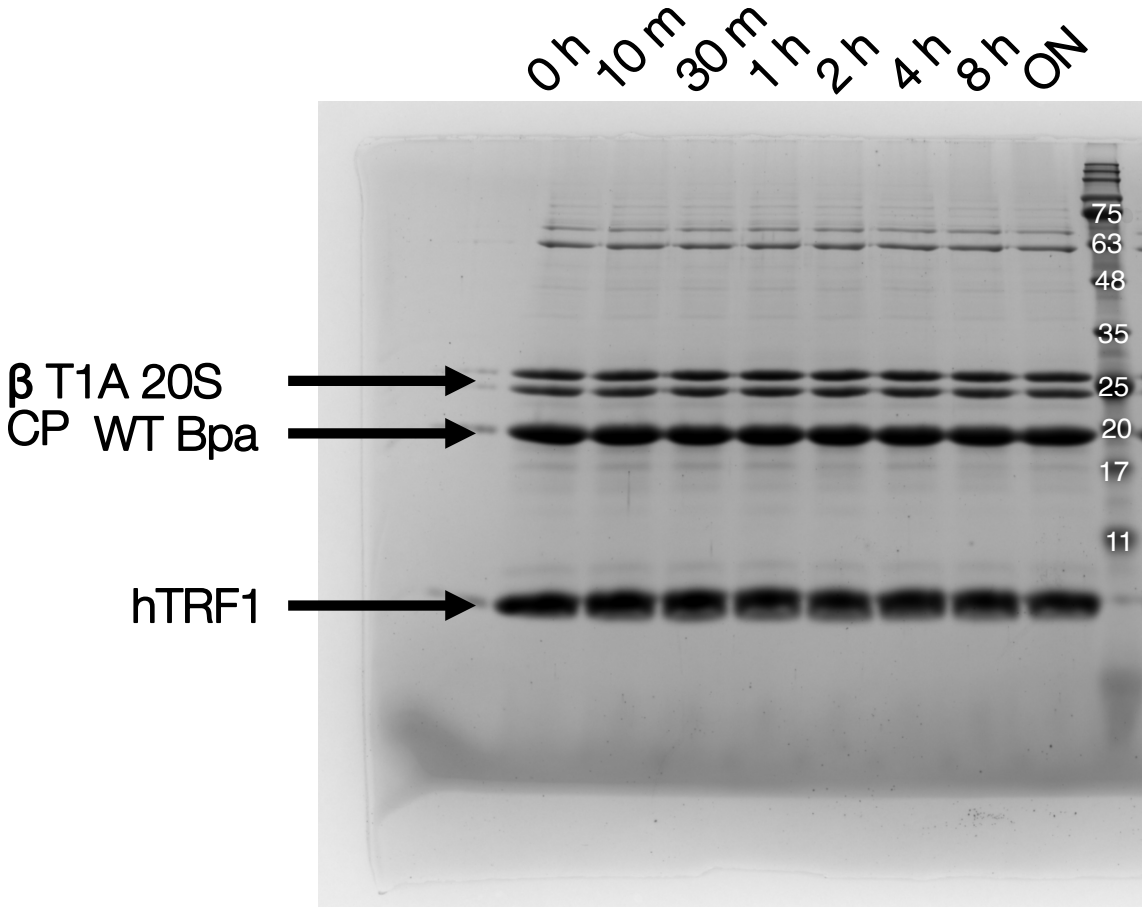

Supplementary Figure 13. hTRF1 is not degraded by the catalytically-inactive 20S CP. All components (WT Bpa, βT1A 20S CP, hTRF1) were combined and incubated at 37 °C for 48 hours. Aliquots were taken at discrete time points (0 h – 48 h) and quenched. Reaction protein concentrations were 0.14 μM 20S CP, 0.8 μM Bpa (dodecamer), and 10 μM hTRF1. Source data are provided as a Source Data file.

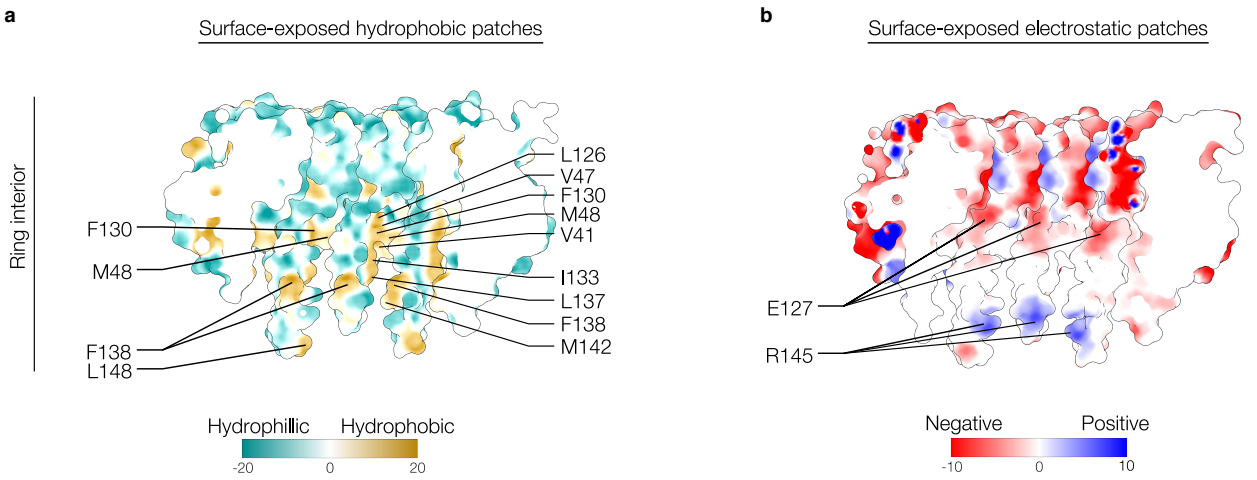

Supplementary Figure 14. Bpa $_{WT}$ surface hydrophobicity and electrostatics. (**a**) Surface-exposed and sequestered hydrophobic patches on the inner-ring of Bpa are shown. Residues contributing to hydrophobicity are labelled and indicated by black lines; (**b**) Surface-exposed and sequestered charged patches for the inner ring of Bpa are shown. Residues contributing to electrostatics are labelled and indicated by black lines. PDB ID: 5LFJ from Bolten *et al.* 2016[3].

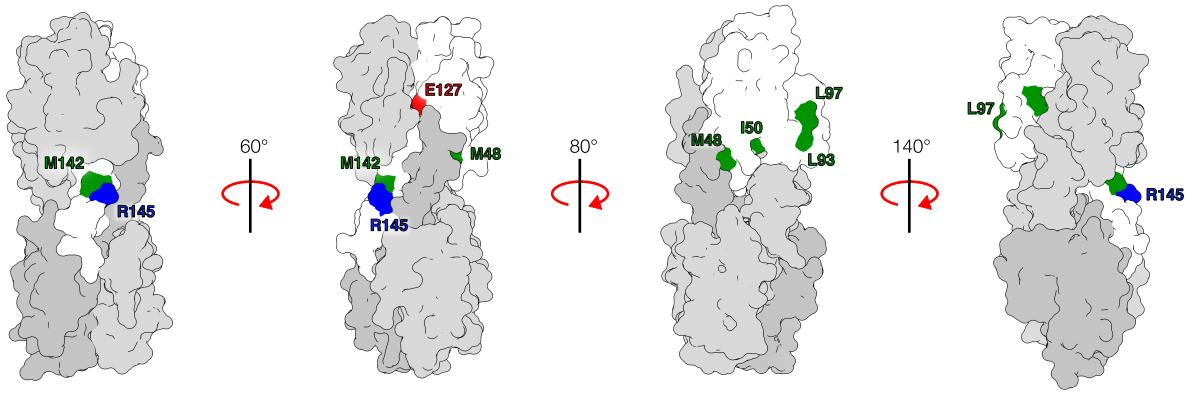

Supplementary Figure 15. Bpa residues involved in hTRF1 binding are sequestered in the tetrameric form. The tetrameric Bpa structure is shown as a surface representation with one monomer highlighted in white (PDB: 5IEU). Green patches correspond to surface-exposed residues that also display chemical shift changes upon addition of hTRF1. Red and blue patches denote electrostatic regions relevant to substrate engagement in the dodecameric form. All colored residues are labeled.

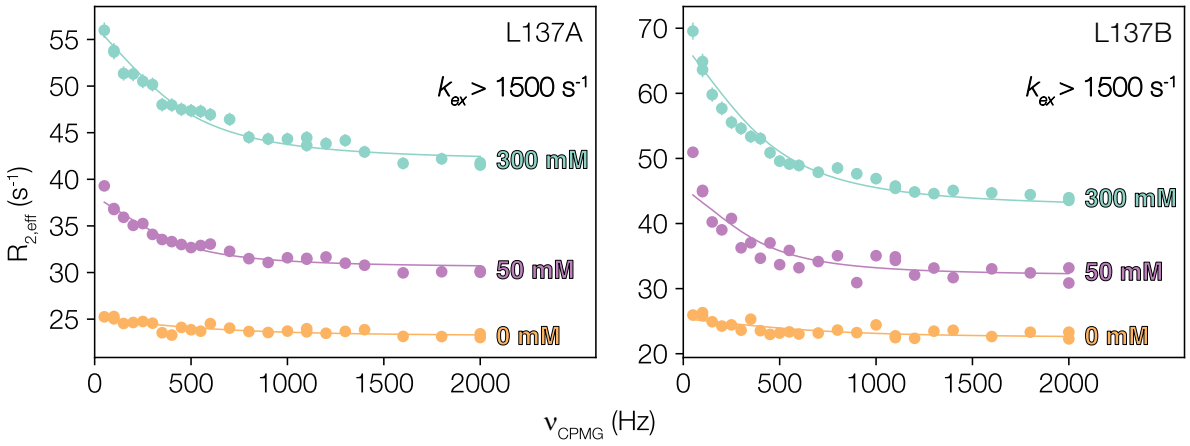

Supplementary Figure 16. {^{13}C-^{1}H} multiple quantum CPMG profiles of Bpa. CPMG profiles for the two methyl groups of L137 (A, left; B, right) at [Bpa] = 900 μM (subunit concentration) and [hTRF1] = 0 μM (orange), 45 μM (purple), and 90 μM (green). Note that the ^{13}C nuclei of the methyl groups of L137 are two of the probes used in chemical shift-based fits of titration profiles to establish hTRF1 binding affinities and stoichiometries (Figure 5).

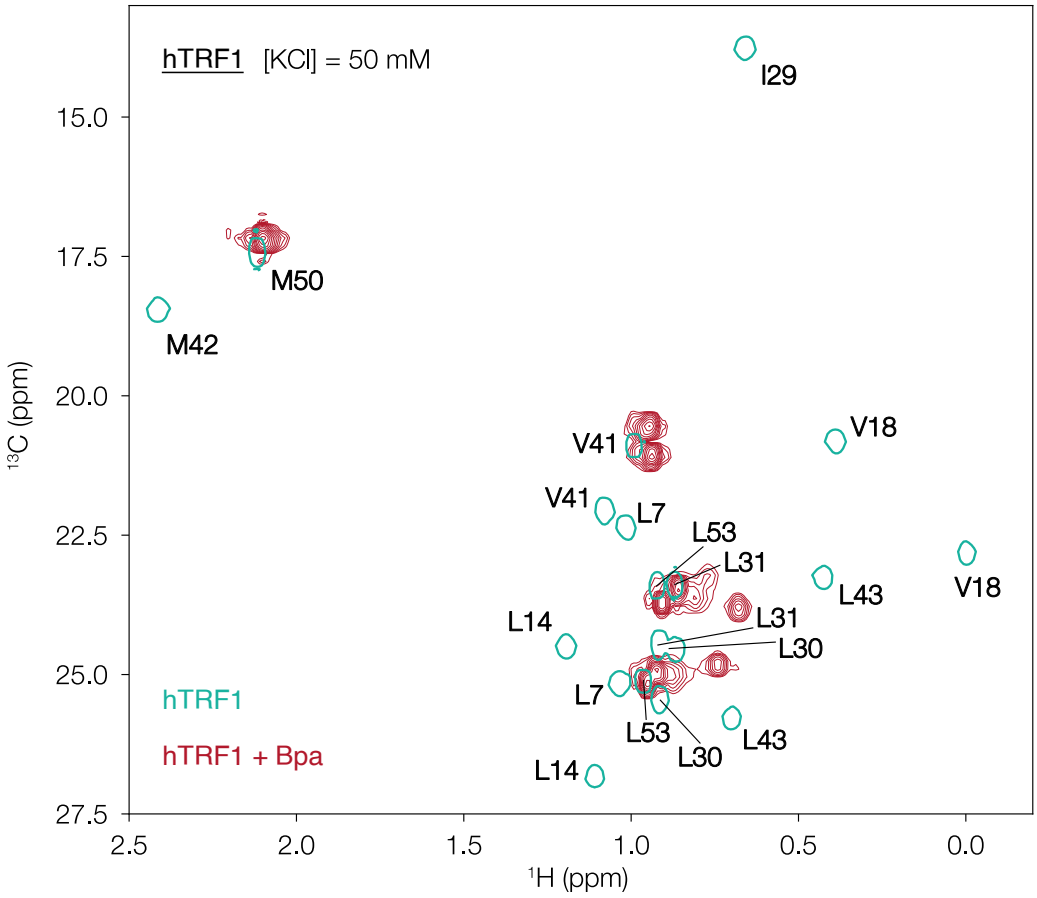

Supplementary Figure 17. hTRF1 is unfolded when bound to Bpa. Superposition of a selected region from ^{1}H-^{13}C HMQC data sets (40 °C, 600 MHz) recorded on samples of ILVM-labeled hTRF1 (turquoise, single contours) and ILVM-labeled hTRF1 in complex with protonated Bpa (red, multiple contours), 50 mM KCl. Note that the spectra of isolated hTRF1 is well-dispersed, while in the chaperone-bound state hTRF1 is only poorly resolved.

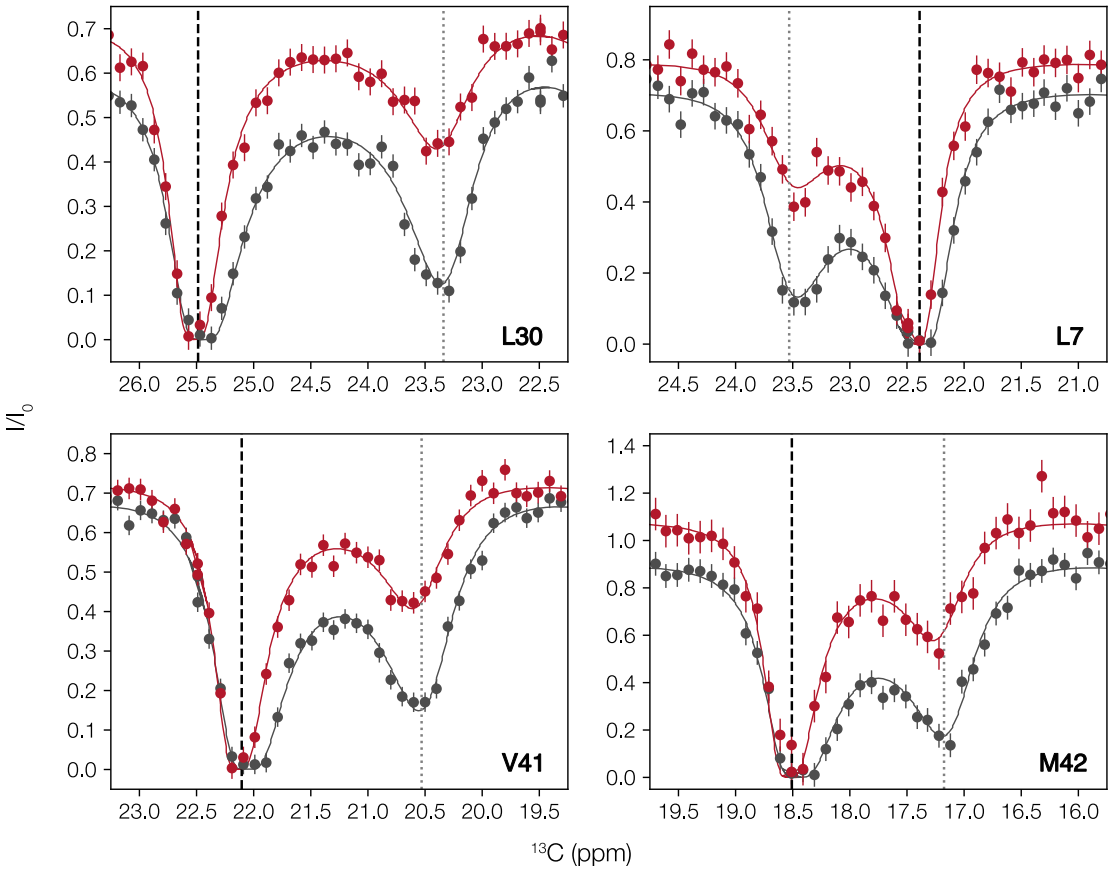

Supplementary Figure 18. Estimation of the unfolded fraction of hTRF1 at 50 and 300 mM KCl, 40 °C. ^{13}C methyl D-CEST profiles[4,5] for four representative methyl groups (denoted on each spectrum) at [KCl] = 50 mM (grey) and 300 mM (red). The chemical shifts of the folded state are indicated by vertical black dashed lines, while those of the unfolded state are indicated by vertical gray dotted lines. Note that the depth of the dips for the unfolded state at high salt (red) are reduced compared to those at low salt (grey), indicating a stabilization of the folded state at the higher ionic strength. Quantitative analysis of the data using the program Chemex[6] indicates a decrease in the unfolded fraction, f^U, from 13.6 ± 0.4% at [KCl] = 50 mM to 7.1 ± 0.3% at [KCl] = 300 mM.

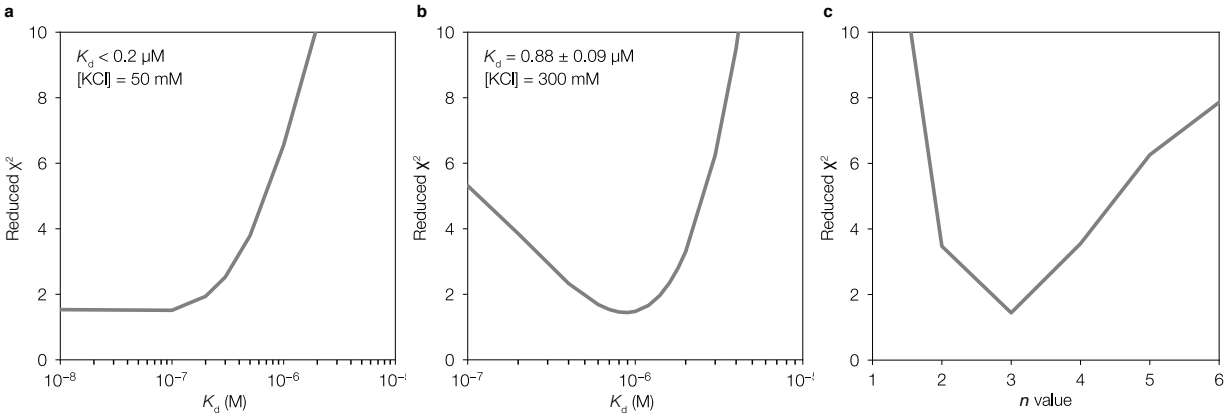

Supplementary Figure 19. Analysis of hTRF1 – Bpa binding via fits of titration profiles. Reduced χ^2 as a function of the microscopic dissociation constant (Eq. 2), K_d, for hTRF1 binding at 50 mM (a) and 300 mM (b) KCl. Values of K_d were obtained from joint fits of all the titration data (both salt concentrations), assuming that the number of bound hTRF1 ligands is independent of salt concentration. A binding model where only the unfolded state of hTRF1 associates with Bpa is assumed. (c) Reduced χ^2 as a function of *n*, establishing that three copies of hTRF1 bind to dodecameric Bpa.

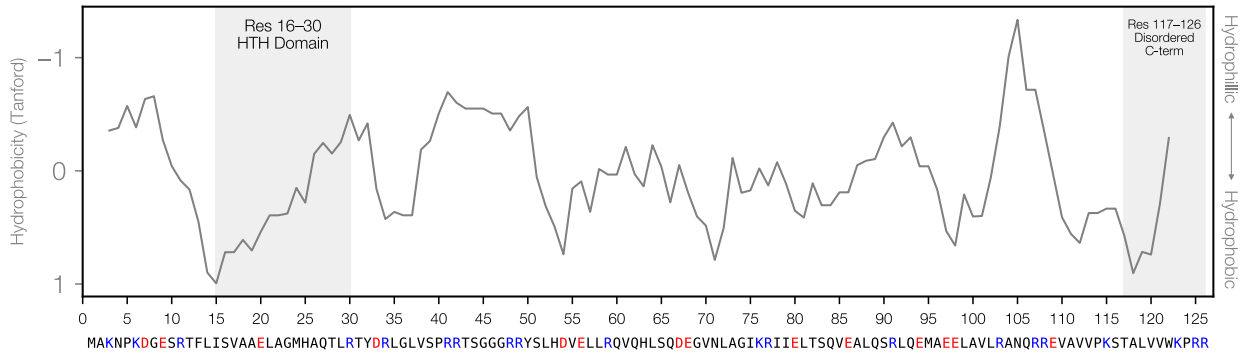

Supplementary Figure 20. Sequence hydrophobicity of HspR. The grey trace indicates the Tanford hydrophobic index for the HspR (Rv0353) sequence. Charged residues are indicated in the sequence using blue (positive) and red (negative). Regions implicated in substrate binding (res 16-30) and 20S CP threading (res 117-126) are indicated by grey shaded panels[7].

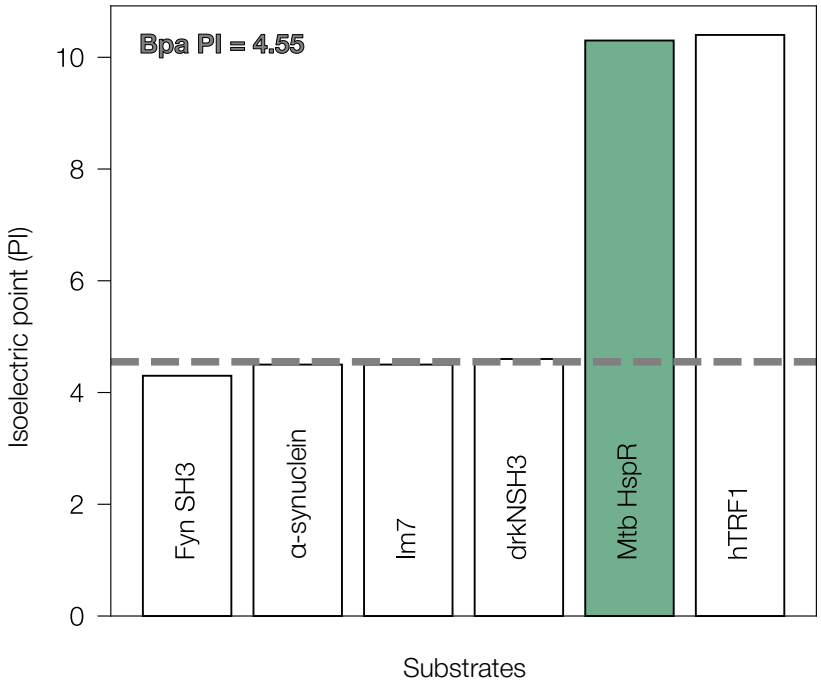

Supplementary Figure 21. Isoelectric point (pI) values for different proteins tested as potential Bpa substrates. Each bar denotes the pI of an experimentally tested or well-established substrate. The green bar denotes HspR, a native substrate of Bpa in *Mtb*. The grey hatched line indicates the pI of Bpa, also shown in the top left corner.

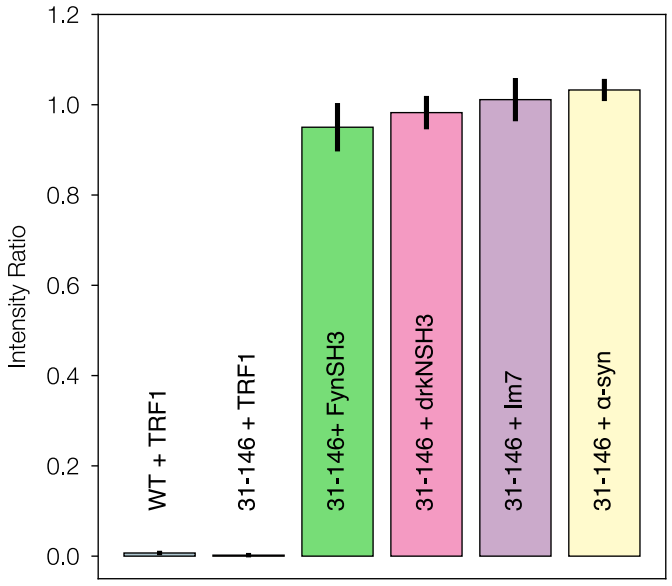

Supplementary Figure 22. Bpa $_{WT}$ and Bpa $_{31\text{-}146}$ substrate screen. NMR peak intensity ratio when Bpa was combined with various substrates. A low peak intensity ratio indicates binding. The Uniprot accession numbers for each substrate are as follows: hTRF1 (P54274, residues 378-430 of the full-length protein), FynSH3 from *Gallus Gallus* (Q05876, residues 85-142, A39V/N53P/V55L mutant[8], drkNSH3 from *Drosophila melanogaster* (Q08012, residues 1-59), lm7 (Q03708), α-syn (P37840).

Supplementary Table 1. Instrument parameters used to record native mass spectra on a Synapt G2Si.

Ion transmission	
ESI capillary voltage	0.7 -1.0 kV
Cone voltage	80 V
Source temperature	30 °C
Desolvation temperature	not applicable
Source offset	80 V
Gas flow	
Cone gas	50 L/h
Desolvation gas	not applicable
Nebulizer gas	not applicable
Trap gas	4.0 mL min^{-1}
Collision energy	
Trap collision energy	0 V
Transfer collision energy	0 V
Trap DC	
Entrance	1 V
Bias	0 V
Trap DC	-2 V
Exit	0 V
IMS DC	
Entrance	-20 V
Helium cell DC	1 V
Helium exit	-20 V
Bias	2 V
Exit	20 V
Transfer DC	
Entrance	5 V
Exit	15 V
Trap and transfer Triwave	
Trap wave velocity	300 m/s
Trap wave height	0.5 V
Transfer wave velocity	247 m/s
Transfer wave height	0.2 V
IMS Triwave	
IMS wave velocity	300 m/s
IMS wave height	40 to 20 V over 100% of IMS duty cycle (linear)
Mobility trapping	
Release time	100 µs
Trap height	15.0 V
Extract height	0 V
Pressures	
Backing	3.07 mBar
Source	7.61×10^{-3} mBar
Trap	1.64×10^{-2} mBar
Helium	2.82×10^{-4} mBar
IMS	3.63×10^{-4} mBar

Transfer	1.46×10^{-2} mBar
TOF	1.15×10^{-6} mBar

Supplementary Table 2. Hydrogen deuterium exchange experimental parameters and resulting statistics.

	Apo Bpa
HDX reaction details	Final D_2O concentration [v/v] 97.5%, pH_{corr} 7.0, 37 °C
HDX time course (sec)	1 h, 2 h, 3 h, 4 h, 5 h, 6 h, 7 h, 8 h, 20 h
Undeuterated controls	3
Back-exchange	33% (value determined by Turner e*t al.* 2025)[9]
Number of peptides	147
Sequence coverage	100%
Average peptide length/redundancy	5.60
Replicates	3 technical replicates
Repeatability	0.15 Da
Significant differences	0.5 Da

References

1. Stivala, A., Wybrow, M., Wirth, A., Whisstock, J. C. & Stuckey, P. J. Automatic generation of protein structure cartoons with Pro-origami. *Bioinformatics* **27**, 3315–3316 (2011).
2. Bai, L. *et al.* Structural analysis of the dodecameric proteasome activator PafE in Mycobacterium tuberculosis. *Proceedings of the National Academy of Sciences* **113**, E1983–E1992 (2016).
3. Bolten, M. *et al.* Structural Analysis of the Bacterial Proteasome Activator Bpa in Complex with the 20S Proteasome. *Structure* **24**, 2138–2151 (2016).
4. Bouvignies, G. & Kay, L. E. A 2D ^{13}C-CEST experiment for studying slowly exchanging protein systems using methyl probes: an application to protein folding. *J Biomol NMR* **53**, 303–310 (2012).
5. Yuwen, T., Kay, L. E. & Bouvignies, G. Dramatic Decrease in CEST Measurement Times Using Multi-Site Excitation. *Chemphyschem* **19**, 1707–1710 (2018).
6. Bouvignies, G. & Kay, L. E. Measurement of Proton Chemical Shifts in Invisible States of Slowly Exchanging Protein Systems by Chemical Exchange Saturation Transfer. *J. Phys. Chem. B* **116**, 14311–14317 (2012).
7. von Rosen, T., Pepelnjak, M., Quast, J.-P., Picotti, P. & Weber-Ban, E. ATP-independent substrate recruitment to proteasomal degradation in mycobacteria. *Life Science Alliance* **6**, (2023).
8. Neudecker, P. *et al.* Identification of a collapsed intermediate with non-native long-range interactions on the folding pathway of a pair of Fyn SH3 domain mutants by NMR relaxation dispersion spectroscopy. *J Mol Biol* **363**, 958–976 (2006).

9. Turner, M. *et al.* Structural basis for allosteric modulation of *M. tuberculosis* proteasome core particle. *Nat Commun* **16**, 3138 (2025).